Radio science for connecting humans to information systems / L'homme connecté

# Compact planar monopole antenna for wearable wireless applications

## Antenne monopole planaire compacte pour les systèmes de communication sans fil portée sur le corps humain

Tsitoha Andriamiharivolamena [a,b,*], Pierre Lemaître-Auger [a], Smail Tedjini [a], Franck Tirard [b]

[a] Université Grenoble Alpes, LCIS, 50, rue Barthélémy-de-Laffemas, 26902 Valence, France
[b] SAFRAN SAGEM, 100, avenue de Paris, 91344 Massy, France

A B S T R A C T

We report in this paper the design and the realization of a compact wearable monopole antenna directly placed over an Artificial Magnetic Conductor (AMC), which is located directly on the body. The major contribution is that there is no space between the monopole and the AMC, or between the AMC and the body. Simulation results and measurements are in good agreement and show that the antenna's performances are as good as the best ones reported so far in the literature, while having a smaller volume. The antenna operates at 1.92 GHz with a bandwidth of 8%. The reflection coefficient of the antenna is −35 dB. The measurement of the antenna gain provides a value of 4.3 dBi with a half-power beamwidth of 70° and a front-to-back radiation ratio of 15.8 dB. Measurement and simulation results also show that the AMC isolates well the monopole from the body: the localized Specific Absorption Rate (SAR) value calculated with 1 g of tissue is 0.34 W/kg with an injected power of 1 W. The antenna with the AMC is well adapted for wearable applications.

© 2015 Published by Elsevier Masson SAS on behalf of Académie des sciences.

R É S U M É

Nous rapportons dans cet article l'étude et la réalisation d'une antenne de type monopole placée directement au-dessus d'un conducteur magnétique artificiel (AMC) sans introduire une couche supplémentaire entre les deux. Les résultats des simulations, qui ont été validés par des mesures, montrent que les performances de l'antenne étudiée sont aussi bonnes que celles rapportées jusqu'à présent. L'antenne fonctionne à 1,92 GHz, avec une bande passante de 8 %. Elle a une adaptation de −35 dB à sa fréquence de résonance. Le gain mesuré de l'antenne est de 4,3 dBi, avec une ouverture à −3 dB de 70° et un rapport entre le rayonnement face avant et le rayonnement face arrière de l'antenne de 15,8 dB. Les résultats des mesures et des simulations montrent que l'AMC permet de bien isoler le monopole du corps. La valeur localisée du débit d'absorption spécifique (DAS) calculée avec

1 g de tissu est 0.34 W/Kg pour une puissance injectée de 1 W. Le dispositif avec l'AMC est très bien adapté à des applications où l'antenne doit être portée directement sur le corps humain.

## 1. Introduction

Nowadays, wireless and wearable systems are more and more considered and expected in almost everyone's life. A lot of people are dreaming to reduce the impact of wearable systems on their mobility by integrating these systems in clothes, including the antenna. But antenna integration close to a body raises the question of body protection against electromagnetic radiations as well as that of the efficiency of the wearable antenna.

Textile patch antenna is one of the solutions proposed in the literature [1–3]. A large ground plane is required to reduce the influence of the human body on the radiation characteristics of the antenna. However, this can enhance surface waves propagating on the ground plane and, thus, modify the radiation pattern and decrease the radiation efficiency. Another solution proposed in the literature to reduce the surface waves, and consequently, to increase the radiation efficiency is a textile cavity-backed slot antenna in a substrate-integrated waveguide (SIW) [4–7]. One very interesting advantage of this antenna is the possibility to integrate directly, into a single substrate, passive and active components. Also, with such technology, dual band antennas [6] or wide band antennas [7] can be achieved. This last point makes the antenna robust towards bending and it also makes its radiation characteristics stable in proximity to the human body [7]. However, a textile cavity-backed slot antenna in SIW requires vias that were put manually up to now. These vias could make the industrialization of such antennas more complicated, and consequently, could raise the manufacturing cost. In addition, textile cavity-backed slot antennas in SIW cannot be placed directly on the body without putting a spacer between the skin and the antenna to isolate the coplanar feed line from the body.

Another solution that attracted a lot of attention in recent years is the use of High-Impedance Surfaces (HIS) [8–12]. Indeed, a HIS placed behind the antenna increases the front-to-back radiation ratio, thus reducing the Specific Absorption Rate (SAR) in the presence of a human body. Besides, such an option was also studied for applications where antennas are placed close to printed circuit boards. In that situation, the HIS reduces the Electromagnetic interference impact on the electronics located on the latter. Moreover, the use of HIS positively contributes to the reduction of the size of the antenna [13].

One of the difficulties when using an antenna close to a HIS is the coupling between the antenna and the HIS structure that results in large modifications of the antenna impedance. This phenomena has been clearly demonstrated in the literature [14,15]. More specifically, the study in [14] showed that a dipole placed at a distance of $0.01\lambda$ above a HIS, where $\lambda$ is the wavelength, has a reflection coefficient less than $-9.54$ dB for phase values of the reflected wave ($\varphi$) comprised between $[-110°, -155°]$ and $[40°, 115°]$. These results were confirmed by the second study [15] for a dipole–HIS distance of $0.02\lambda$. The main conclusion of those studies is that a dipole close to a HIS has a low reflection coefficient when the impedance of the HIS is finite and purely imaginary (this impedance is defined as the ratio between the tangential electric and the magnetic fields on the surface of the structure). In this specific case, the HIS is a called Reactive Impedance Surface (RIS). This was theoretically shown in [16] thanks to the image theory: the minimal coupling between a dipole and its image is obtained when the HIS becomes a RIS.

The previous results were obtained for dipole antennas. However, in practice, the realization of dipole antennas close to a RIS on fabrics is difficult because of the presence of vias and baluns. Monopole antennas seem to be simpler to realize on fabrics. They were recently used close to HIS without any via [8–10]. However, in all studies reported so far, an additional spacer made out of foam (1 to 2 mm thick) was required to obtain a good antenna adaptation. In this paper, we will show that it is possible to obtain very good radiation performances with a monopole antenna placed over a HIS without the need of an additional spacer, i.e. the antenna substrate is directly placed over the patch structure of the HIS. In the present study, the antenna is designed for wearable military applications working at 2.06 GHz. The HIS operates at its resonance frequency and, for that reason, it is called an Artificial Magnetic Conductor (AMC) [17]. The volume of the antenna and the AMC structure presented here is one of the smallest (relative to the wavelength) reported so far.

The paper is organized as follows. The principle of HIS is developed in Section 2. Then, the design of a HIS based on a mushroom structure without via is presented in Section 3. After that, results of a planar monopole placed directly over an AMC are compared with numerical simulations in Section 4. In Section 5, we present the results of a planar monopole antenna over an AMC placed directly on arm. Finally, concluding remarks are reported in the last section.

## 2. Principle of a HIS

### 2.1. Performances of a dipole antenna placed close to a human body

In order to understand the behavior of an antenna in the presence of the human body, the radiation emitted by a dipole antenna placed close to a human body was simulated thanks to a commercial full-wave electromagnetic simulator
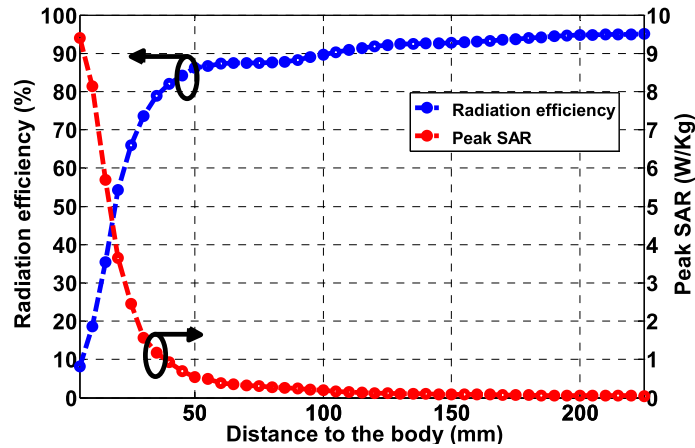
**Fig. 1.** (Color online.) Variation of the antenna efficiency and of the SAR with respect to the distance between the antenna and the body. SAR is computed with a power of 1 W for 10 g of tissue.

(CST Microwave Studio). The dipole is fed symmetrically at the center by a discrete port with an operating frequency of 2 GHz and a characteristic impedance of 50 Ω. The human model "Voxel Family (Gustav)" of CST Microwave Studio is used in this study. The separation distance between the body and the dipole, $d$, is the parametric variable of the study.

The results show that the radiation characteristics of the dipole are modified when it is placed very close to the body, see Fig. 1. Indeed, for $d = 1$ cm, the resonant frequency is shifted by 1.6% toward the higher frequencies. The radiation pattern is also modified: the main advantage of using an omnidirectional antenna to cover all the space is no more possible. Moreover, the radiation efficiency, $\eta_r$, decreases drastically (less than 17%) and the localized SAR values calculated for 1 g and 10 g of tissue are greatly increased, up to 17 W/kg and 8 W/kg, respectively, for an injected power of 1 W. It is worth noting that these values are much greater than the accepted limit values: 1.6 W/kg for 1 g of tissue [18] and 2 W/kg for 10 g of tissue [19,20]. In the opposite, when $d$ increases, the efficiency of the antenna increases and the SAR values decrease. For example, the radiation efficiency becomes 86% and the SAR values are lower than the accepted limit values for $d = 5$ cm. Therefore, for that separation distance of 5 cm, the antenna operates correctly and body exposition to the electromagnetic wave is acceptable, but antenna integration into clothing is not possible anymore. It is obvious that a separation device is needed behind the dipole to isolate it from the body.

### 2.2. HIS ground plane

A simple ground plane cannot be used to protect a human body from the radiation of an antenna for two reasons. First, the phase shift of an electromagnetic wave reflecting on it is $\pi$. Thus, the ground plane must be placed at a distance $\lambda/4$ from the antenna to create a constructive interference. If the antenna is located too close to the ground plane, the antenna's impedance becomes very low, and impedance matching becomes very difficult to achieve; all the electromagnetic energy is stored in the near field and the quality factor of the antenna increases [16]. The second reason is the presence of surface waves on the ground plane. These waves will propagate until they meet a discontinuity where they will radiate. Thus, side-lobes appear in the radiation pattern.

Another type of ground plane must then be used, like a HIS. A HIS is a structure with a surface impedance that has a complex value (purely reactive in the ideal case) and that varies with frequency [16]. The first characteristic of a HIS is to have a reflection phase which varies from 180° to −180° depending on the frequency. At the resonant frequency of the HIS, the phase reflection is equal to 0°. In this case, the HIS acts as a Perfect Magnetic Conductor (PMC), also called Artificial Magnetic Conductor (AMC). Therefore, the antenna can be placed close to the AMC because the current of the antenna and its image current are both in phase. The image current enhances the radiation in front of the antenna. This makes the antenna quite easy to be integrated into clothing and to be placed close to a human body.

The second characteristic of a HIS is to have, in some cases, a frequency band where no surface waves can propagate. In this case, the HIS has an Electromagnetic Band Gap (EBG) behavior [21]. This characteristic blocks surface waves on the antenna substrate, thus resulting in a good directivity of the antenna.

The third desired characteristic of the HIS is angular stability [22]. Indeed, the characterization of the reflection coefficient of the HIS is obtained with a normal incidence wave. However, when the antenna is placed close to the HIS, the incidence angle of the wave is not necessarily normal to the surface of the HIS. Ideally, characteristics of the HIS should be independent of the incidence angle and also of the polarization of the incident wave.
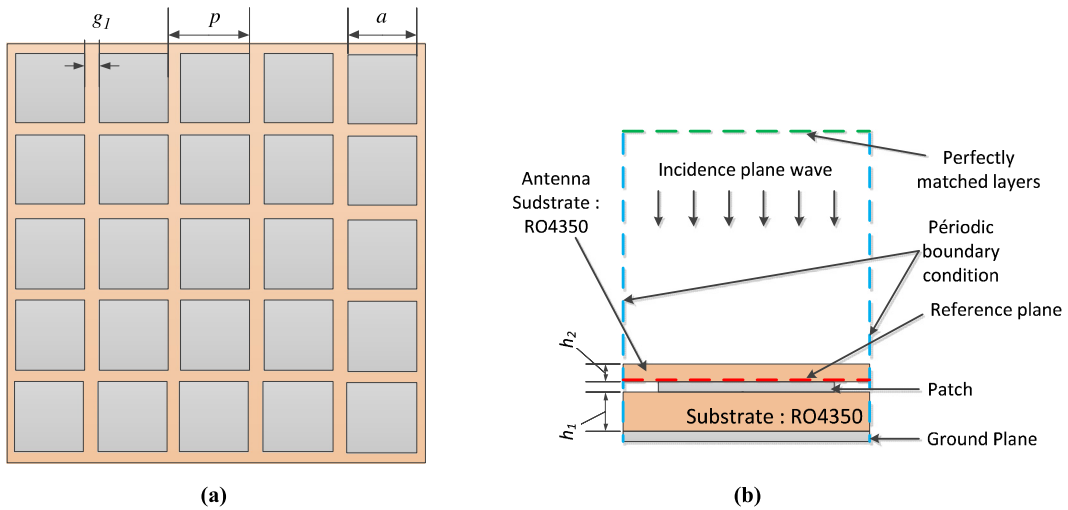
**Fig. 2.** (Color online.) Structure of the mushroom without via composed by $5 \times 5$ cells. The overall dimensions of the structure are: 86.5 mm $\times$ 86.5 mm. (a) Top view of the HIS. (b) Side view of one cell of the HIS with the antenna substrate. Also illustrated: boundary conditions used for the simulations.

## 3. Design of a HIS based on a mushroom structure without via

The HIS based on the "mushroom" topology proposed in [23] is one of the most used structures in the literature. But, unfortunately, the realization of this structure into clothing would be quite complex because of the presence of vias. However, results reported in [17] showed that a mushroom-HIS without via has a wider bandwidth (19.35%) than other types of HIS topologies, like cross, meandered cell, or interdigited patch. Moreover, the AMC and EBG behaviors of this structure can overlap in the same frequency band [21] by increasing the period of the structure. Furthermore, the angular stability of this structure was studied in [22]. The results showed that the angular stability can be optimized by reducing the ratio between the width of the patch and the periodicity of the structure. The mushroom without via topology was thus chosen for the present study.

Fig. 2a shows the structure of the mushroom without via. Essentially, it is a network of square metallic patches periodically placed on a 3.2-mm-thick RO4350 substrate ($\varepsilon_r = 3.66$ and $\tan \delta = 0.004$). The conductor used is 16-µm-thick copper. The width of the patch is $a$ and the gap between two patches is $g_1$. The periodicity of the structure is $p$. A ground plane is located under the substrate. No via between the patches and the ground plane is used. Therefore, the structure is cheap to realize and well adapted to integration on fabrics.

We used the simple model proposed in [23] to design the mushroom structure: the equivalent circuit is composed of a capacitor, $C$, in parallel with an inductor, $L$. The expression of the surface impedance is given by the following formula:

$$Z = \frac{Z_L Z_C}{Z_L + Z_C} = \frac{jL\omega}{1 - LC\omega^2} \tag{1}$$

where $Z_L$ is the impedance of the inductor and $Z_C$ is the impedance of the capacitor, given by:

$$C = \frac{a\varepsilon_0(\varepsilon_r + 1)}{\pi} \cosh^{-1}\left(\frac{p + a}{p - a}\right) \tag{2}$$

and:

$$L = \mu_0 h_1 \tag{3}$$

where $h_1$ is the thickness of the substrate; $\varepsilon_0$ and $\mu_0$ are the permittivity and the permeability of the free space. Thus, the resonance frequency is:

$$f_0 = \frac{1}{2\pi \sqrt{LC}} = \frac{1}{2\pi \sqrt{\mu_0 h_1 \frac{a\varepsilon_0(\varepsilon_r + 1)}{\pi} \cosh^{-1}(\frac{2a + g_1}{g_1})}} \tag{4}$$

More accurate models are proposed in [16,24], but the simple LC model is sufficient as a first step of the design. Indeed, an optimization step using a full-wave simulator is always needed whatever the model used.

In the first step of the design, a value of $g_1$ is chosen, taking into account the physical limit imposed by the fabrication process. In the present case, $g_1$ is fixed to 0.3 mm. Then, from (4), the value of $a$ is computed for the desired frequency. After that, the HIS structure is simulated with the substrate that will be used for the antenna. The latter is placed immediately

**Table 1**

Dimensions of the HIS and of the monopole alone.

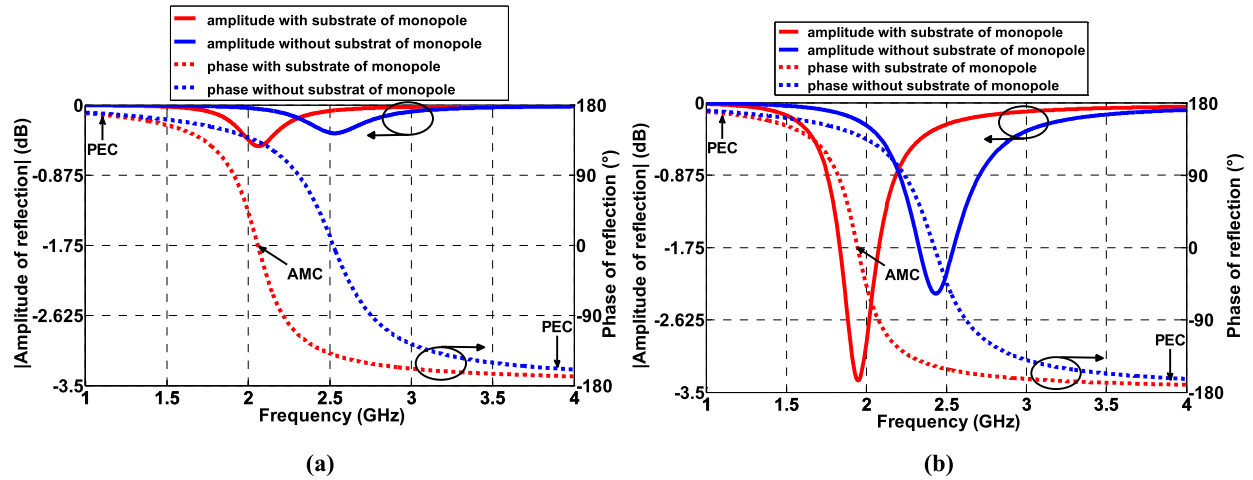| Parameter | Value (mm) | Parameter | Value (mm) | Parameter | Value (mm) |
|-----------|-----------|-----------|-----------|-----------|-----------|
| $W$ | 3 | $\ell$ | 28.2 | $p$ | 17.3 |
| $g_1 = g_2$ | 0.3 | $L$ | 27.75($L_0$) | $a$ | 17 |
| $d$ | 25 | $h_2$ | 1.6 | $h_1$ | 3.2 |



**Fig. 3.** (Color online.) Simulated reflection coefficient of the mushroom without via obtained with a normal incidence wave. (a) Substrate RO4350. (b) Substrate FR4.

above the HIS, like it is shown in Fig. 2b [11]. This is done because the influence of this substrate has a great impact on the resonant frequency of the HIS. Thus, taking into account its impact on the HIS design at the beginning of the design process will greatly facilitate the integration of the antenna over the HIS in the next design step.

The optimal value of $a$ is found thanks to the full-wave simulations. The dimensions of the HIS after optimization are given in Table 1.

The reflection coefficient of the HIS obtained by simulation is shown in Fig. 3a. Like mentioned previously, we observe that the presence of the antenna substrate has a significant effect on the reflection coefficient: amplitude and phase curves are both shifted to lower frequencies. The phase of the reflection coefficient, $\varphi$, varies from $-180°$ to $180°$. When $\varphi$ is equal to $180°$ or $-180°$, the mushroom acts as a perfect-electric-conductor (PEC) ground plane. Its surface impedance is equal to $0\ \Omega$ and the amplitude of the reflection coefficient is equal to 1 (0 dB). At 2.06 GHz, $\varphi$ is equal to $0°$, the mushroom acts as an AMC ground plane, and its surface impedance is infinite. However, the amplitude of the reflection coefficient is $-0.5$ dB. For other values of $\varphi$, the surface impedance of the mushroom is a purely imaginary value: the mushroom acts as a RIS. In this case, the losses are low but the interference is not totally constructive. Therefore, the gain of the antenna will decrease. The performances of the AMC and RIS will be discussed in Section 4.

The angular stability of the HIS was also studied by illuminating the structure with an oblique incidence illumination. The incidence angle, $\theta$, is varied from $0°$ to $50°$ for both TE and TM polarizations. The reflection coefficient of the HIS obtained thanks to the simulations is shown in Fig. 4. The results show that the HIS is not sensitive for TE polarization. For TM polarization, the shift of the resonance frequency toward the higher frequencies is lower than 6% when $\theta$ is equal to $40°$ and reaches 9% at $50°$.

## 4. Planar monopole antenna over the HIS

### 4.1. Design of the planar monopole antenna

The antenna used is a monopole fed by a coplanar transmission line, like it is shown in Fig. 5a. The substrate and the metal are the same as the ones used for the HIS realization, the thickness of the substrate is $h_2$. First, the monopole alone is designed to operate correctly at 2.06 GHz. The dimensions of the monopole antenna thus obtained are given in Table 1. The reflection coefficient of the monopole alone (with length $L_0$) is shown in Fig. 6. The monopole has an acceptable matching: $-20$ dB. The calculated value of the radiation efficiency is 98%.
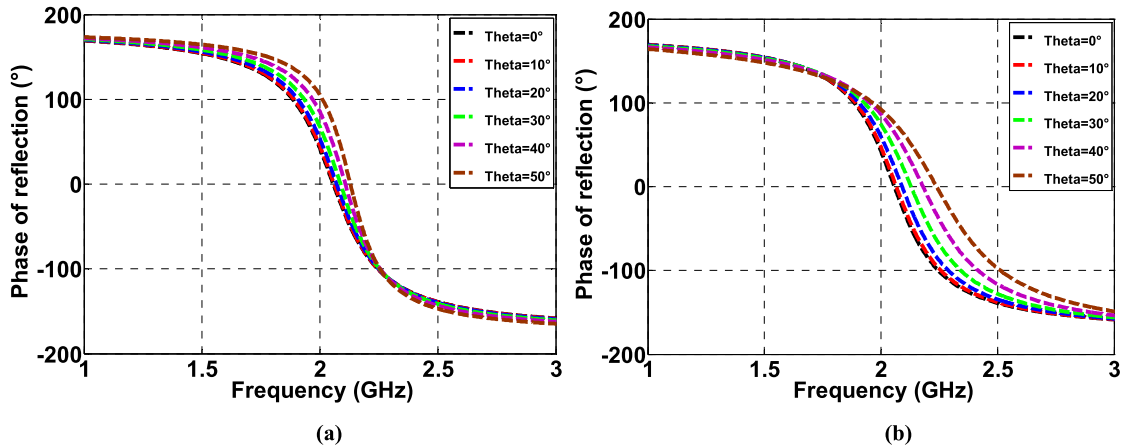
Fig. 4. (Color online.) Simulated reflection coefficient of the mushroom without via obtained with an oblique incidence illumination. $\theta$ is varied from $0°$ to $50°$. (a) TE polarization. (b) TM polarization.
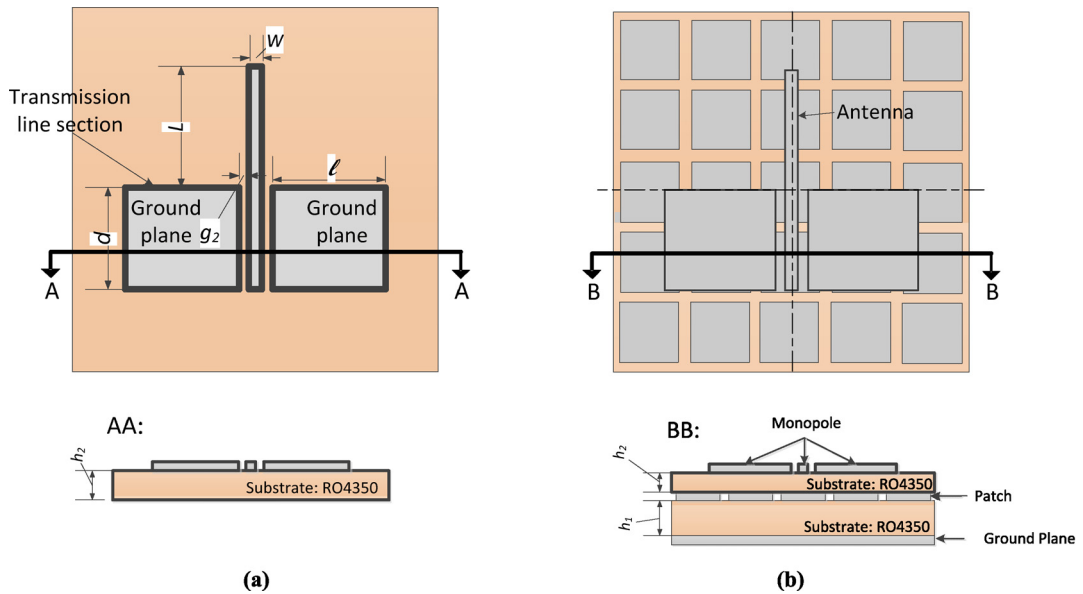


Fig. 5. (Color online.) (a) Monopole antenna alone, $L = L_0$. (b) Monopole over HIS, $L = L_2$.

### 4.2. Design of the planar monopole antenna over the HIS

Then, the monopole is placed directly over a HIS made of $5 \times 5$ cells. Fig. 5b shows the structure of the antenna placed over the HIS. The beginning of the monopole is centered with respect to the HIS. It is worth noting that no additional spacer is inserted between the patch of the mushroom and the monopole substrate, contrarily to several published works [8–10], thanks to the procedure described in the previous section.

The technique explained in [15] for a dipole is used here to design the monopole antenna over the HIS. Only the length $L$ of the monopole is varied. A good matching of $-53$ dB is obtained at 2.06 GHz for a monopole length $L_2$ as shown in Fig. 6 after optimization.

Fig. 7 shows the evolution of the reflection coefficient of the monopole placed over the HSI for several values of $L$. It can be seen that there are three frequency bands for which the monopole has a good impedance matching: [1.75–1.87] GHz, [2–2.18] GHz and [2.22–2.31] GHz. These frequency bands correspond to phase values of the reflected wave: $\varphi_1 = [104°, 131°]$, $\varphi_2 = [-76°, 42°]$ and $\varphi_3 = [-115°, -92°]$. The best reflection coefficient is obtained for the monopole length: $L = L_2 = 26.25$ mm ($f = 2.06$ GHz, the desired frequency), like it is shown in Fig. 8. This frequency corresponds exactly to the resonance frequency of the AMC. It is interesting to note that another value of phase shift, corresponding to different values of the frequency, would also give good results. For example, the $L_1$ curve in Fig. 8 represents the best reflection coefficient of the monopole in Band 1. Its resonance frequency is $f_1 = 1.82$ GHz. At this frequency, the HIS has a RIS behavior. In Bands 1 and 2, it was checked from simulations that the HIS always had an EBG behavior. Finally, in Band 3, the monopole having a length $L_3 = 23.25$ mm has the best reflection coefficient. This occurs at 2.25 GHz. At this frequency,
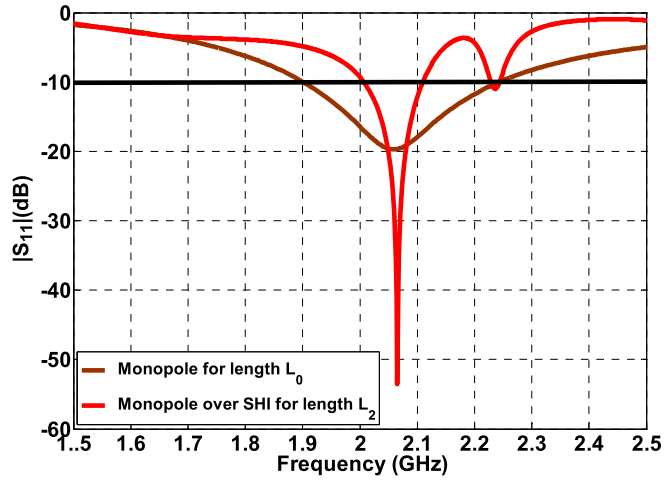
**Fig. 6.** (Color online.) Simulated reflection coefficient of the monopole. $L_0 = 27.75$ mm and $L_2 = 26.25$ mm.
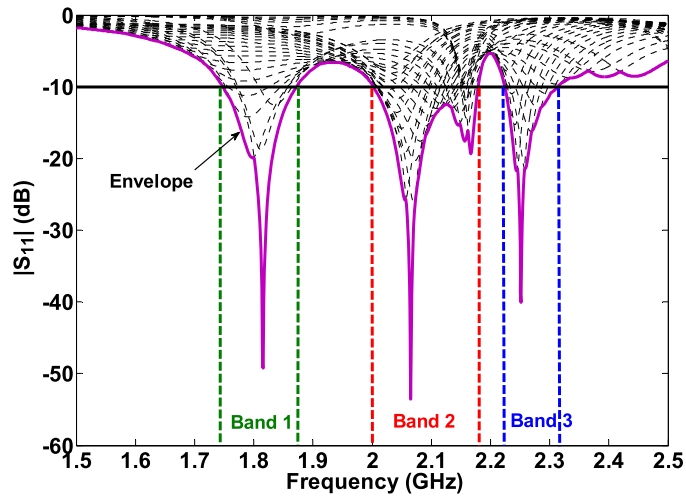


**Fig. 7.** (Color online.) Evolution of the reflection coefficient of the monopole placed over the HIS for several values of $L$.
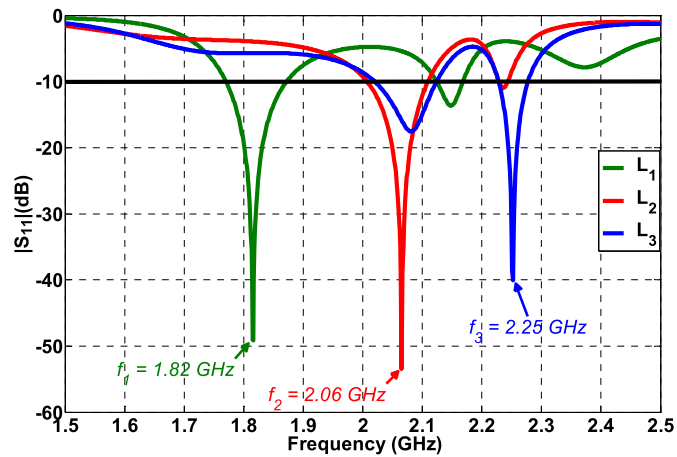


**Fig. 8.** (Color online.) Best reflection coefficient of the monopole placed over the HIS in the three frequency bands.

**Table 2**

Performances of the three best monopole placed directly over the HIS in the three bands shown in Fig. 7.

| L (mm) | $|S_{11}|$ (dB) | f (GHz) | Bandwidth (%) | Gain (dBi) | $\eta_r$ (%) | Behavior |
|---|---|---|---|---|---|---|
| $L_1 = 16.25$ | −49 | 1.82 | 5.5 | 6.7 | 93 | RIS/EBG |
| $L_2 = 26.25$ | −53 | 2.06 | 5.3 | 7 | 92 | AMC/EBG |
| $L_3 = 23.25$ | −40 | 2.25 | 2.2 | 3.2 | 83 | RIS |
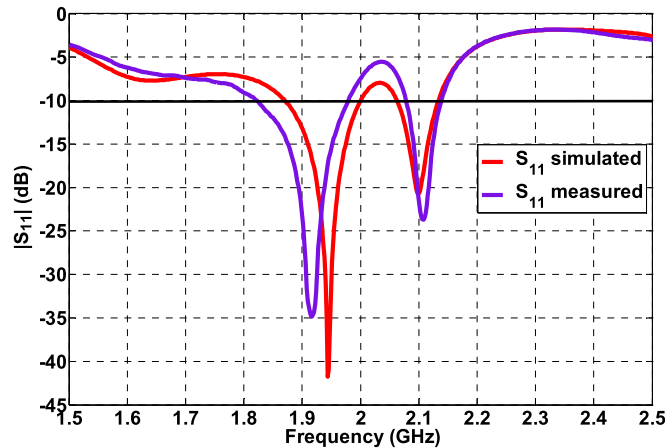


**Fig. 9.** (Color online.) Simulated and measured reflection coefficients in free space.

the HIS has a RIS behavior, but it was observed that the radiation pattern presents side lobes due to the presence of surface waves. The EBG behavior is not present anymore. The performances of the three monopoles corresponding to lengths $L_1$, $L_2$ and $L_3$ are given in Table 2.

The AMC plane is the best candidate for the monopole in terms of impedance matching and realized gain. In terms of bandwidth and radiation efficiency, the best candidate is in Band 1. However, the performances of both monopoles (1 and 2) are very close. The radiation efficiency of monopole 2 is decreased by the losses in the AMC. Indeed, there is a 1% difference between the radiation efficiency of monopole 1 compared to the one of monopole 2.

### 4.3. Simulation and measurement results in free space

For cost reasons, a first prototype was realized on the FR4 ($\varepsilon_r = 4.3$ and $\tan \delta = 0.01$) substrate instead of the RO4350. Thickness is unchanged. The thickness, the size and the dimensions of the HIS have not been modified. Therefore, the resonance frequency of the AMC is shifted towards lower frequencies: 1.94 GHz instead of 2.06 GHz, see Fig. 3b. Also, the thickness and the dimensions of the monopole have not been modified, except for the length $L$. With the same technique used to optimize the monopole-HIS with the RO4350 substrate, a good impedance matching with a 6.6% bandwidth was achieved at the resonance frequency of the AMC (1.94 GHz). The new length $L_2$ of the monopole is 22.25 mm.

Fig. 9 shows the measured reflection coefficient. Good agreement is obtained between simulation and measurement. The measured resonance frequency value is 1.92 GHz compared to 1.94 GHz predicted by simulation (a 1% difference). The antenna has a very good impedance matching. The measured reflection coefficient is −35 dB. This is better than the one obtained in [8–10]. The measured bandwidth is 8%. This is two times wider than the one obtained in [10].

The radiation pattern of the antenna was also measured (at 1.92 GHz). Fig. 10 shows the comparison between measurement and simulation results. Good agreement is obtained between both. The measured gain value is 4.3 dBi. This is similar to the one (4.8 dBi) obtained in [9]. The measured front to back ratio of the antenna is 15.8 dB. This value is the twice of the one obtained in [9] while the size (relative to the wavelength) of the HIS of the antenna is equivalent to the one proposed in [9], see Table 3.

## 5. Planar monopole antenna over an AMC placed directly on the arm

The antenna was finally characterized when it is placed directly over an arm; see Fig. 11a. There is no space between the antenna and the arm. Fig. 11b shows the comparison between the measured reflection coefficient and the one obtained in free space. The two results are very close. The resonance frequency and the bandwidth of the antenna are not sensitive to the presence of the body. This demonstrates that the AMC isolates well the antenna from the body. The latter is thus well protected.

The radiation pattern was also measured. They results are compared to the simulation. Fig. 12a shows that a good agreement is obtained between the two results. Fig. 12b shows the comparison between the measured radiation pattern
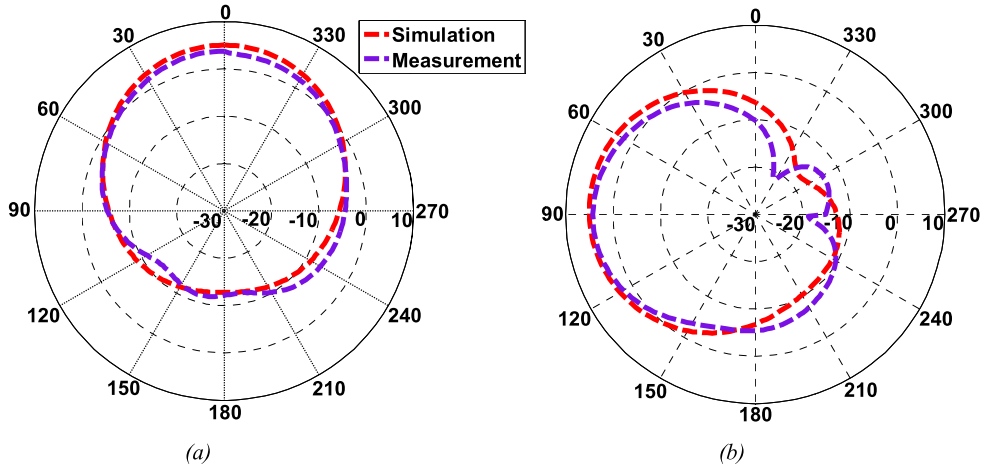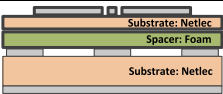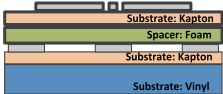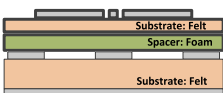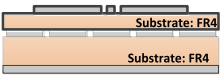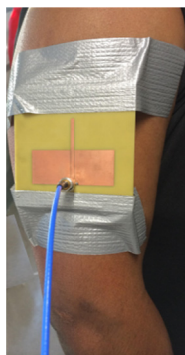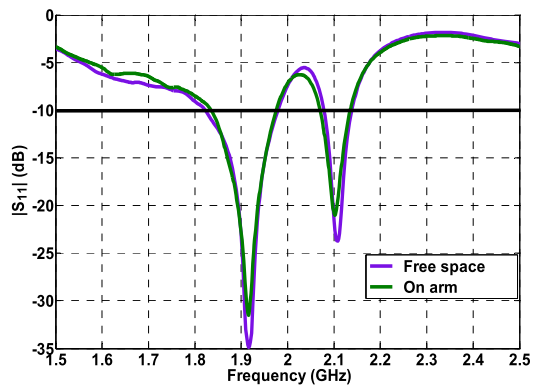
**Fig. 10.** (Color online.) Simulated and measured radiation pattern in free space at 1.92 GHz. (a) *H*-Plane. (b) *E*-Plane.

**Table 3**
Dimensions and volume of antennas placed over a HIS.

| References | Antenna cross section | $f$ | Dimensions | | | Volume |
|---|---|---|---|---|---|---|
| | | | Length | Width | Thickness | |
| [8] | | 2.45 GHz | 85.5 mm | 85.5 mm | 5.7 mm | 41 668.425 mm$^3$ |
| | | | 0.698$\lambda$ | 0.698$\lambda$ | 0.046$\lambda$ | 0.023$\lambda^3$ |
| [9] | | 2.45 GHz | 65.7 mm | 65.7 mm | 3.3 mm | 14 244.417 mm$^3$ |
| | | | 0.536$\lambda$ | 0.536$\lambda$ | 0.027$\lambda$ | 0.008$\lambda^3$ |
| [10] | | 2.45 GHz | 120 mm | 120 mm | 4.3 mm | 61 920 mm$^3$ |
| | | | 0.98$\lambda$ | 0.98$\lambda$ | 0.035$\lambda$ | 0.034$\lambda^3$ |
| Proposed antenna | | 1.92 GHz | 86.5 mm | 86.5 mm | 4.8 mm | 35 171.328 mm$^3$ |
| | | | 0.554$\lambda$ | 0.554$\lambda$ | 0.031$\lambda$ | 0.009$\lambda^3$ |



**Fig. 11.** (Color online.) (a) Monopole over the AMC placed directly on the arm. (b) Measured reflection coefficient.
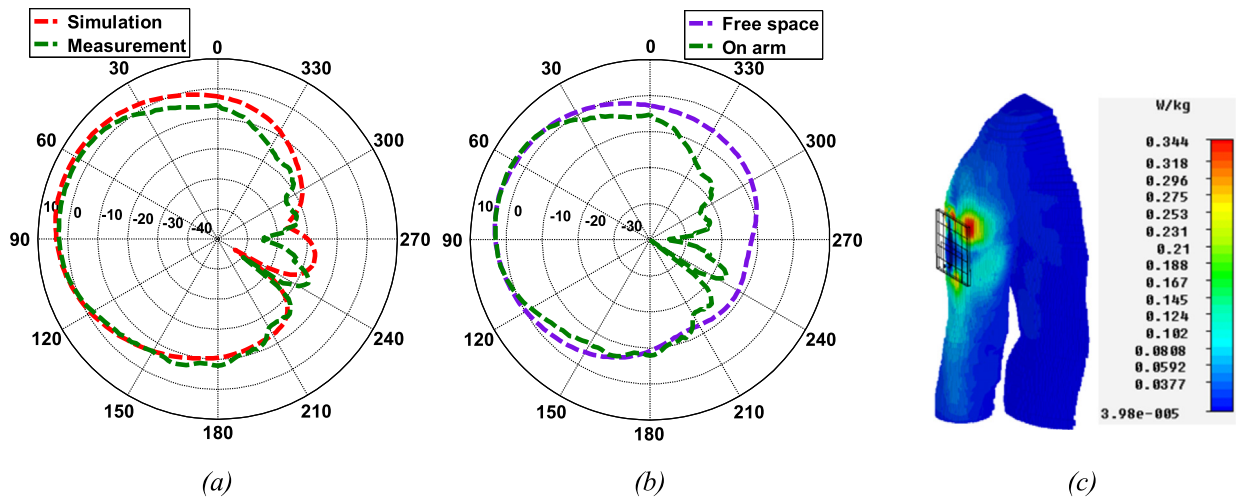
**Fig. 12.** (Color online.) Radiation pattern in the *E*-Plane. (a) Comparison between simulated and measured radiation patterns. (b) Comparison between results obtained in free space and the ones obtained when the antenna is placed directly on the arm. (c) Calculated SAR.

in free space and the one obtained in the presence of the body. There is no change for the zone in front of the antenna. However, the front to back ratio value is increased to 25 dB. This indicates that the body absorbs the radiated energy behind the antenna. However, this energy is very low. Indeed, simulations presented in Fig. 12(c) show the localization of the power absorbed. Calculated localized SAR values with 1 g and 10 g of tissue are 0.34 W/kg and 0.18 W/kg respectively for an injected power of 1 W. Those values are below European standards (1.6 W/kg and 2 W/kg). The value obtained with 1 g of tissue is a half of the one obtained in [9] while the injected power is 0.125 W. This demonstrates that the AMC used in this study protects well the body from the radiation of the monopole.

## 6. Conclusion

A monopole antenna directly placed over a HIS was presented. The design procedure is explained. It was found that simulating the HIS with the substrate of the antenna but without the latter at the very beginning of the conception makes it easy and eliminates the need for an extra spacer between the HIS and the antenna. It was also found that a phase shift of zero corresponding to the AMC behavior of the HIS gives the best results, but that another phase shift could also give good results. The AMC conditions are thus not the only possible solution for such application. Finally, the volume obtained with the proposed antenna prototype is one of the smallest reported so far, and the performances obtained are as good as, or even better than, the results reported up to now.

The antenna and the HIS were designed for wearable wireless applications, but were tested with FR4 substrate. Nevertheless, dimensions obtained are compatible with inkjet printing or screen printing technologies for future realization with conductive ink on fabrics.

## Acknowledgements

## References

[1] C. Hertleer, H. Rogier, L. Vallozzi, L. Van Langenhove, A textile antenna for off-body communication integrated into protective clothing for firefighters, IEEE Trans. Antennas Propag. 57 (4) (2009) 919–925.
[2] E.K. Kaivanto, M. Berg, E. Salonen, P. de Maagt, Wearable circularly polarized antenna for personal satellite communication and navigation, IEEE Trans. Antennas Propag. 59 (12) (2011) 4490–4496.
[3] K. Koski, L. Sydanheimo, Y. Rahmat-Samii, L. Ukkonen, Fundamental characteristics of electro-textiles in wearable UHF RFID patch antennas for body-centric sensing systems, IEEE Trans. Antennas Propag. 62 (12) (2014) 6454–6462.
[4] R. Moro, S. Agneessens, H. Rogier, M. Bozzi, Wearable textile antenna in substrate integrated waveguide technology, Electron. Lett. 48 (16) (2012) 985–987.
[5] R. Moro, M. Bozzi, S. Agneessens, H. Rogier, Compact cavity-backed antenna on textile in substrate integrated waveguide (SIW) technology, in: Proceedings of the European Microwave Conference, EuMC, 2013, pp. 1007–1010.
[6] S. Agneessens, S. Lemey, R. Moro, M. Bozzi, H. Rogier, The next generation textile antennas based on substrate integrated waveguide technology, in: Gen. Assem. Sci. Symp. XXXIst URSI, URSI GASS 2014, 2014, pp. 1–4.
[7] S. Lemey, F. Declercq, H. Rogier, Dual-band substrate integrated waveguide textile antenna with integrated solar harvester, IEEE Antennas Wirel. Propag. Lett. 13 (2014) 269–272.

[8]  M. Mantash, A.-C. Tarot, S. Collardey, K. Mahdjoubi, Investigation of flexible textile antennas and AMC reflectors, Int. J. Antennas Propag. 2012 (2012) 236505, 10 pp.

[9]  H.R. Raad, A.I. Abbosh, H.M. Al-Rizzo, D.G. Rucker, Flexible and compact AMC based antenna for telemedicine applications, IEEE Trans. Antennas Propag. 61 (2) (2013) 524–531.

[10] Shaozhen Zhu, R. Langley, Dual-band wearable textile antenna on an EBG substrate, IEEE Trans. Antennas Propag. 57 (4) (2009) 926–935.

[11] Jaehoon Kim, Y. Rahmat-Samii, Low-profile loop antenna above EBG structure, in: Antennas and Propagation Society International Symposium, vol. 2A, 2005 IEEE, 2005, pp. 570–573.

[12] S. Kim, Y.-J. Ren, H. Lee, A. Rida, S. Nikolaou, M.M. Tentzeris, Monopole antenna with inkjet-printed EBG array on paper substrate for wearable applications, IEEE Antenn. Wireless Propag. Lett. 11 (2012) 663–666.

[13] F. Yang, A. Aminian, Y. Rahmat-Samii, A novel surface-wave antenna design using a thin periodically loaded ground plane, Microw. Opt. Technol. Lett. 47 (3) (2005) 240–245.

[14] M.F. Abedin, M. Ali, Effects of EBG reflection phase profiles on the input impedance and bandwidth of ultrathin directional dipoles, IEE Trans. Antenn. Propag. 53 (11) (2005) 3664–3672.

[15] Fan Yang, Y. Rahmat-Samii, Reflection phase characterizations of the EBG ground plane for low profile wire antenna applications, IEE Trans. Antenn. Propag. 51 (10) (2003) 2691–2703.

[16] H. Mosallaei, K. Sarabandi, Antenna miniaturization and bandwidth enhancement using a reactive impedance substrate, IEE Trans. Antenn. Propag. 52 (9) (2004) 2403–2414.

[17] F. Costa, S. Genovesi, A. Monorchio, On the bandwidth of high-impedance frequency selective surfaces, IEEE Antenn. Wireless Propag. Lett. 8 (2009) 1341–1344.

[18] F. C. Commission, Evaluating compliance with FCC guidelines for human exposure to radiofrequency electromagnetic fields, DC, tech. rep., suppl. C to OET Bull. 65. Office of Engineering and Technology, Federal Communications Commission, Washington, DC, 2001.

[19] I. Guideline, Guidelines for limiting exposure to time-varying electric, magnetic, and electromagnetic fields (up to 300 GHz), Health Phys 74 (4) (1998) 494–522.

[20] I. C. on N.-I. R. Protection, ICNIRP statement on the "Guidelines for limiting exposure to time-varying electric, magnetic, and electromagnetic fields (up to 300 GHz)", Health Phys. 97 (3) (2009) 257–258.

[21] G. Goussetis, A.P. Feresidis, J.C. Vardaxoglou, Tailoring the AMC and EBG characteristics of periodic metallic arrays printed on grounded dielectric substrate, IEE Trans. Antenn. Propag. 54 (1) (2006) 82–89.

[22] P. Kovács, Z. Raida, M. Martínez-Vázquez, Parametric study of mushroom-like and planar periodic structures in terms of simultaneous AMC and EBG properties, Radioengineering 17 (4) (2008) 19–24.

[23] D. Sievenpiper, Lijun Zhang, R.F.J. Broas, N.G. Alexopolous, E. Yablonovitch, High-impedance electromagnetic surfaces with a forbidden frequency band, IEEE Trans. Microw. Theory Techn. 47 (11) (1999) 2059–2074.

[24] S.A. Tretyakov, C.R. Simovski, Dynamic model of artificial reactive impedance surfaces, J. Electromagn. Waves Appl. 17 (1) (2003) 131–145.